J|A|C|S
ARTICLES
Published on Web 04/17/2002

Stepwise Charge Separation and Charge Recombination in Ferrocene-*meso*,*meso*-Linked Porphyrin Dimer−Fullerene Triad

Hiroshi Imahori,* Koichi Tamaki,‡ Yasuyuki Araki,§ Yuji Sekiguchi,# Osamu Ito,*,§ Yoshiteru Sakata,‡ and Shunichi Fukuzumi*,#

Contribution from the Department of Molecular Engineering, Graduate School of Engineering, Kyoto University, CREST, Japan Science and Technology Corporation (JST), Sakyo-ku, Kyoto 606-8501, Japan, The Institute of Scientific and Industrial Research, Osaka University, 8-1 Mihoga-oka, Ibaraki, Osaka 567-0047, Japan, the Institute of Multidisciplinary Research for Advanced Materials, Tohoku University, CREST, Japan Science and Technology Corporation (JST), Sendai, Miyagi 980-8577, Japan, and the Department of Material and Life Science, Graduate School of Engineering, Osaka University, CREST, Japan Science and Technology Corporation (JST), Suita, Osaka 565-0871, Japan

Received July 19, 2001. Revised Manuscript Received March 11, 2002

Abstract: *A meso,meso*-linked porphyrin dimer [$(ZnP)_2$] as a light-harvesting chromophore has been incorporated into a photosynthetic multistep electron-transfer model for the first time, including ferrocene (Fc), as an electron donor and fullerene (C_{60}) as an electron acceptor to construct the ferrocene-*meso*,*meso*-linked porphyrin dimer−fullerene system (Fc−$(ZnP)_2$−C_{60}). Photoirradiation of Fc−$(ZnP)_2$−C_{60} results in photoinduced electron transfer from the singlet excited state of the porphyrin dimer [$^1(ZnP)_2$*] to the C_{60} moiety to produce the porphyrin dimer radical cation−C_{60} radical anion pair, Fc−$(ZnP)_2^{\bullet+}$−$C_{60}^{\bullet-}$. In competition with the back electron transfer from $C_{60}^{\bullet-}$ to $(ZnP)_2^{\bullet+}$ to the ground state, an electron transfer from Fc to $(ZnP)_2^{\bullet+}$ occurs to give the final charge-separated (CS) state, that is, Fc$^+$−$(ZnP)_2$−$C_{60}^{\bullet-}$, which is detected as the transient absorption spectra by the laser flash photolysis. The quantum yield of formation of the final CS state is determined as 0.80 in benzonitrile. The final CS state decays obeying first-order kinetics with a lifetime of 19 μs in benzonitrile at 295 K. The activation energy for the charge recombination (CR) process is determined as 0.15 eV in benzonitrile, which is much larger than the value expected from the direct CR process to the ground state. This value is rather comparable to the energy difference between the initial CS state (Fc−$(ZnP)_2^{\bullet+}$−$C_{60}^{\bullet-}$) and the final CS state (Fc$^+$−$(ZnP)_2$−$C_{60}^{\bullet-}$). This indicates that the back electron transfer to the ground state occurs via the reversed stepwise processes,that is, a rate-limiting electron transfer from $(ZnP)_2$ to Fc$^+$ to give the initial CS state (Fc−$(ZnP)_2^{\bullet+}$−$C_{60}^{\bullet-}$), followed by a fast electron transfer from $C_{60}^{\bullet-}$ to $(ZnP)_2^{\bullet+}$ to regenerate the ground state, Fc−$(ZnP)_2$−C_{60}. This is in sharp contrast with the extremely slow direct CR process of bacteriochlorophyll dimer radical cation−quinone radical anion pair in bacterial reaction centers.

Introduction

Investigations of photoinduced electron transfer (ET) in donor−acceptor-linked molecules have attracted enormous interest. Investigators have been motivated by the desire to address basic mechanistic problems on ET chemistry and biology as well as to develop artificial photosynthetic systems for light energy conversion.[1−10] Natural photosynthesis in the purple bacterial reaction centers employs a multistep ET strategy to realize the efficient conversion of light energy to chemical energy.[11] Namely, energy is absorbed by the dimer of bacteriochlorophyll (Bchl) molecules, generating its singlet excited

* To whom correspondence should be addressed. E-mails: imahori@mee3.moleng.kyoto-u.ac.jp, ito@tagen.tohoku.ac.jp, fukuzumi@chem.eng.osaka-u.ac.jp.
† Kyoto University.
‡ The Institute of Scientific and Industrial Research, Osaka University.
§ Tohoku University.
# Graduate School of Engineering, Osaka University.

(1) (a) Marcus, R. A.; Sutin, N. *Biochim. Biophys. Acta* **1985**, *811*, 265. (b) Marcus, R. A. *Angew. Chem. Int. Ed. Engl.* **1993**, *32*, 1111. (c) Bixon, M.; Jortner, J. *Adv. Chem. Phys.* **1999**, *106*, 35. (d) Newton, M. D. *Chem. Rev.* **1991**, *91*, 767.
(2) (a) Winkler, J. R.; Gray, H. B. *Chem. Rev.* **1992**, *92*, 369. (b) Moser, C. C.; Keske, J. M.; Warncke, K.; Farid, R. S.; Dutton, P. L. *Nature* **1992**, *355*, 796. (c) Kirmaier, C.; Holton, D. In *The Photosynthetic Reaction Center*; Deisenhofer, J., Norris, J. R., Eds.; Academic Press: San Diego, 1993; Vol. II, pp 49−70. (d) Langen, R.; Chang, I.-J.; Germanas, J. P.; Richards, J. H.; Winkler, J. R.; Gray, H. B. *Science* **1995**, *268*, 1733. (e) Page, C. C.; Moser, C. C.; Chen, X.; Dutton, P. L. *Nature* **1999**, *402*, 47.
(3) (a) Willner, I. *Acc. Chem. Res.* **1997**, *30*, 347. (b) McLendon, G.; Hake, R. *Chem. Rev.* **1992**, *92*, 481. (c) Lewis, F. D.; Letsinger, R. L.; Wasielewski, M. R. *Acc. Chem. Res.* **2001**, *34*, 159.
(4) (a) Gould, I. R.; Farid, S. *Acc. Chem. Res.* **1996**, *29*, 522. (b) Mataga, N.; Miyasaka, H. *Adv. Chem. Phys.* **1999**, *107*, 431.
(5) (a) Miller, J. R.; Calcaterra, L. T.; Closs, G. L. *J. Am. Chem. Soc.* **1984**, *106*, 3047. (b) Closs, G. L.; Miller, J. R. *Science* **1988**, *240*, 440. (c) Barbara, P. F.; Meyer, T. J.; Ratner, M. A. *J. Phys. Chem.* **1996**, *100*, 13148.
(6) (a) Connolly, J. S.; Bolton, J. R. In *Photoinduced Electron Transfer*; Fox, M. A., Chanon, M., Eds.; Elsevier: Amsterdam, 1988; Part D, pp 303−393. (b) Wasielewski, M. R. In *Photoinduced Electron Transfer*; Fox, M. A., Chanon, M., Eds.; Elsevier: Amsterdam, 1988; Part A, pp 161−206.

state (^{1}(Bchl)$_2$*), which lies ~1.4 eV above the ground state. Within ~3 ps, an ET occurs from ^{1}(Bchl)$_2$* to the bacteriopheophytin (Bphe) molecule located ~9 Å (= R_{ee}, edge-to-edge distance) distant via a two-step sequential mechanism or a one-step superexchange mechanism. The energy of (Bchl)$_2^{\bullet+}$Bphe$^{\bullet-}$ (~1.2 eV) is lowered by ~0.2 eV, which matches well the reorganization energy (λ) of ET to optimize the forward ET process; but the charge recombination (CR) process is shifted deeply into the inverted region of Marcus parabola to retard the CR process. In a subsequent charge-shift (CSH) step, an electron is transferred in ~200 ps from Bphe$^{\bullet-}$ to the primary quinone Q_A, over an R_{ee} value of ~9 Å. This reaction yields the charge-separated (CS) state of (Bchl)$_2^{\bullet+}Q_A^{\bullet-}$, which lies only ~0.6 eV above the ground state. This means that the energy as large as 0.8 eV is lost to obtain the CS state. In a final isoenergetic step, an ET takes place from $Q_A^{\bullet-}$ to Q_B, with a time constant of ~100 μs. The resulting final CS state with a lifetime of ~1 s across the membrane eventually leads to the production of chemical energy. Although the quantum efficiency of the production of (Bchl)$_2^{\bullet+}Q_B^{\bullet-}$ is ~100%, the energy efficiency (~40%) is not perfect. There may be plenty of room for improvement of the energy efficiency while optimizing the charge separation efficiency as well as the CS lifetime. Such optimization is important to develop artificial photosynthetic systems that can convert solar energy into chemical and electrical energies more efficiently than natural systems.

Fullerenes have exhibited unique ET properties as acceptors in donor−acceptor-linked systems.[12−23] In particular, the small reorganization energies make it possible to accelerate photoinduced charge separation and CSH and, on the other hand, to decelerate CR processes relative to comparable systems in which two-dimensional acceptors, such as quinones and imides are employed.[13] Such a remarkable effect can be ascribed to the delocalization of charge spread over the three-dimensional framework of fullerenes, in addition to the rigid structure in both the ground and excited states. Thus, utilization of fullerenes in donor−acceptor-linked systems allows us to realize the optimization of ET processes, such as photosynthesis, regardless of the surrounding environment (i.e., solvents).[22] However, the light-harvesting efficiency remains to be improved.

We report herein incorporation of *meso,meso*-linked porphyrin dimer [(ZnP)$_2$] as an improved light-harvesting chromophore, as compared to the monomer porphyrin, into a photosynthetic ET model to construct the ferrocene-*meso,meso*-linked porphyrin dimer−fullerene triad (Fc−(ZnP)$_2$−C_{60}), where the C_{60} and the ferrocene (Fc) are tethered at both the ends of (ZnP)$_2$, as shown in Figure 1. We previously reported that Fc−ZnP−C_{60} (Figure 1) reveals photoinduced charge separation from the porphyrin excited singlet state to C_{60}, followed by a charge shift (CSH), leading to the production of final CS state (i.e., ferricenium ion (Fc^+)−C_{60} radical anion ($C_{60}^{\bullet-}$) pair) with an extremely high quantum yield (nearly unity) as well as with a lifetime of up to 16 μs.[22c−e] The edge-to-edge distance of the Fc^+−ZnP−$C_{60}^{\bullet-}$ radical ion pair (R_{ee} = 30.3 Å) is enlarged in the Fc^+−(ZnP)$_2$−

(7) (a) Wasielewski, M. R. *Chem. Rev.* **1992**, *92*, 435. (b) Bixon, M.; Fajer, J.; Feher, G.; Freed, J. H.; Gamliel, D.; Hoff, A. J.; Levanon, H.; Möbius, D.; Norris, J. R.; Nechushtai, R.; Scherz, A.; Sessler, J. L.; Stehlik, D. H. A. *Isr. J. Chem.* **1992**, *32*, 369. (c) Gust, D.; Moore, T. A.; Moore, A. L. *Acc. Chem. Res.* **1993**, *26*, 198. (d) Kurreck, H.; Huber, M. *Angew. Chem., Int. Ed. Engl.* **1995**, *34*, 849. (e) Gust, D.; Moore, T. A.; Moore, A. L. *Acc. Chem. Res.* **2001**, *34*, 40.

(8) (a) Harriman, A.; Sauvage, J.-P. *Chem. Soc. Rev.* **1996**, *26*, 41. (b) Blanco, M.-J.; Jiménez, M. C.; Chambron, J.-C.; Heitz, V.; Linke, M.; Sauvage, J.-P. *Chem. Soc. Rev.* **1999**, *28*, 293. (c) Balzani, V.; Juris, A.; Venturi, M.; Campagna, S.; Serroni, S. *Chem. Rev.* **1996**, *96*, 759. (d) *Electron Transfer in Chemistry*; Balzani, V. Ed.; Wiley-VCH: Weinheim, 2001.

(9) (a) Paddon-Row, M. N. *Acc. Chem. Res.* **1994**, *27*, 18. (b) Verhoeven, J. W. *Adv. Chem. Phys.* **1999**, *106*, 603. (c) Maruyama, K.; Osuka, A.; Mataga, N. *Pure Appl. Chem.* **1994**, *66*, 867. (d) Osuka, A.; Mataga, N.; Okada, T. *Pure Appl. Chem.* **1997**, *69*, 797. (e) Sun, L.; Hammarström, L.; Åkermark, B.; Styring, S. *Chem. Soc. Rev.* **2001**, *30*, 36.

(10) (a) Imahori, H.; Sakata, Y. *Adv. Mater.* **1997**, *9*, 537. (b) Imahori, H.; Sakata, Y. *Eur. J. Org. Chem.* **1999**, 2445. (c) Guldi, D. M. *Chem. Commun.* **2000**, 321. (d) Guldi, D. M.; Prato, M. *Acc. Chem. Res.* **2000**, *33*, 695.

(11) (a) *The Photosynthetic Reaction Center*; Deisenhofer, J., Norris, J. R., Ed.; Academic Press: San Diego, 1993. (b) *Anoxygenic Photosynthetic Bacteria*; Blankenship, R. E., Madigan, M. T., Bauer, C. E., Eds.; Kluwer Academic Publishing: Dordrecht, 1995.

(12) (a) Martín, N.; Sánchez, L.; Illescas, B.; Pérez, I. *Chem. Rev.* **1998**, *98*, 2527. (b) Prato, M. *J. Mater. Chem.* **1997**, *7*, 1097. (c) Diederich, F.; Gómez-López, M. *Chem. Soc. Rev.* **1999**, *28*, 263. (d) Guldi, D. M.; Kamat, P. V. In *Fullerenes*; Kadish, K. M., Ruoff, R. S., Eds.; John Wiley & Sons: New York, 2000; Chapter 5, pp 225−281.

(13) (a) Imahori, H.; Hagiwara, K.; Akiyama, T.; Aoki, M.; Taniguchi, S.; Okada, T.; Shirakawa, M.; Sakata, Y. *Chem. Phys. Lett.* **1996**, *263*, 545. (b) Imahori, H.; Tkachenko, N. V.; Vehmanen, V.; Tamaki, K.; Lemmetyinen, H.; Sakata, Y.; Fukuzumi, S. *J. Phys. Chem. A* **2001**, *105*, 1750. (c) Vehmanen, V.; Tkachenko, N. V.; Imahori, H.; Fukuzumi, S.; Lemmetyinen, H. *Spectrochim. Acta, Part A* **2001**, 57, 2229.

(14) Guldi, D. M.; Asmus, K.-D. *J. Am. Chem. Soc.* **1997**, *119*, 5744.

(15) (a) Liddell, P. A.; Sumida, J. P.; Macpherson, A. N.; Noss, L.; Seely, G. R.; Clark, K. N.; Moore, A. L.; Moore, T. A.; Gust, D. *Photochem. Photobiol.* **1994**, *60*, 537. (b) Liddell, P. A.; Kuciauskas, D.; Sumida, J. P.; Nash, B.; Nguyen, D.; Moore, A. L.; Moore, T. A.; Gust, D. *J. Am. Chem. Soc.* **1997**, *119*, 1400. (c) Kuciauskas, D.; Liddell, P. A.; Lin, S.; Johnson, T. E.; Weghorn, S. J.; Lindsey, J. S.; Moore, A. L.; Moore, T. A.; Gust, D. *J. Am. Chem. Soc.* **1999**, *121*, 8604.

(16) (a) Williams, R. M.; Zwier, J. M.; Verhoeven, J. W. *J. Am. Chem. Soc.* **1995**, *117*, 4093. (b) Williams, R. M.; Koeberg, M.; Lawson, J. M.; An, Y.-Z.; Rubin, Y.; Paddon-Row, M. N.; Verhoeven, J. W. *J. Org. Chem.* **1996**, *61*, 5055. (c) Bell, T. D. M.; Smith, T. A.; Ghiggino, K. P.; Ranasinghe, M. G.; Shephard, M. J.; Paddon-Row, M. N. *Chem. Phys. Lett.* **1997**, *268*, 223.

(17) (a) Baran, P. S.; Monaco, R. R.; Khan, A. U.; Schuster, D. I.; Wilson, S. R. *J. Am. Chem. Soc.* **1997**, *119*, 8363. (b) Schuster, D. I.; Cheng, P.; Wilson, S. R.; Prokhorenko, V.; Katterle, M.; Holzwarth, A. R.; Braslavsky, S. E.; Klihm, G.; Williams, R. M.; Luo, C. *J. Am. Chem. Soc.* **1999**, *121*, 11599. (c) Sun, Y.; Wilson, S. R.; Schuster, D. I. *J. Am. Chem. Soc.* **2001**, *123*, 5348.

(18) (a) Armspach, D.; Constable, E. C.; Diederich, F.; Housecroft, C. E.; Nierengarten, J.-F. *Chem. Eur. J.* **1998**, *4*, 723. (b) Camps, X.; Dietel, E.; Hirsch, A.; Pyo, S.; Echegoyen, L.; Hackbarth, S.; Röder, B. *Chem. Eur. J.* **1999**, *5*, 2362. (c) Armaroli, N.; Marconi, G.; Echegoyen, L.; Bourgeois, J.-P.; Diederich, F. *Chem. Eur. J.* **2000**, *6*, 1629. (d) van Hal, P. A.; Knol, J.; Langeveld-Voss, B. M. W.; Meskers, S. C. J.; Hummelen, J. C.; Janssen, R. A. J. *J. Phys. Chem. A* **2000**, *104*, 5974. (e) Eckert, J.-F.; Nicoud, J.-F.; Nierengarten, J.-F.; Liu, S.-G.; Echegoyen, L.; Barigelletti, F.; Armaroli, N.; Ouali, L.; Krasnikov, V.; Hadziioannou, G. *J. Am. Chem. Soc.* **2000**, *122*, 7467.

(19) (a) Thomas, K. G.; Biju, V.; Guldi, D. M.; Kamat, P. V.; George, M. V. *J. Phys. Chem. B* **1999**, *103*, 8864. (b) Tkachenko, N. V.; Rantala, L.; Tauber, A. Y.; Helaja, J.; Hynninen, P. H.; Lemmetyinen, H. *J. Am. Chem. Soc.* **1999**, *121*, 9378. (c) Tkachenko, N. V.; Vuorimaa, E.; Kesti, T.; Alekseev, A. S.; Tauber, A. Y.; Hynninen, P. H.; Lemmetyinen, H. *J. Phys. Chem. B* **2000**, *104*, 6371. (d) D'Souza, F.; Deviprasad, G. R.; El-Khouly, M. E.; Fujitsuka, M.; Ito, O. *J. Am. Chem. Soc.* **2001**, *123*, 5277. (e) Kamat, P. V.; Barazzouk, S.; Hotchandani, S.; Thomas, K. G. *Chem. Eur. J.* **2000**, *6*, 3914.

(20) (a) Guldi, D. M.; Maggini, M.; Scorrano, G.; Prato, M. *J. Am. Chem. Soc.* **1997**, *119*, 974. (b) Polese, A.; Mondini, S.; Bianco, A.; Toniolo, C.; Scorrano, G.; Guldi, D. M.; Maggini, M. *J. Am. Chem. Soc.* **1999**, *121*, 3446. (c) Guldi, D. M.; Luo, C.; Prato, M.; Troisi, A.; Zerbetto, F.; Scheloske, M.; Dietel, E.; Bauer, W.; Hirsch, A. *J. Am. Chem. Soc.* **2001**, *123*, 9166.

(21) (a) Imahori, H.; Hagiwara, K.; Akiyama, T.; Taniguchi, S.; Okada, T.; Sakata, Y. *Chem. Lett.* **1995**, 265. (b) Imahori, H.; Hagiwara, K.; Aoki, M.; Akiyama, T.; Taniguchi, S.; Okada, T.; Shirakawa, M.; Sakata, Y. *J. Am. Chem. Soc.* **1996**, *118*, 11771. (c) Imahori, H.; El-Khouly, M. E.; Fujitsuka, M.; Ito, O.; Sakata, Y.; Fukuzumi, S. *J. Phys. Chem. A* **2001**, *105*, 325.

(22) (a) Imahori, H.; Yamada, K.; Hasegawa, M.; Taniguchi, S.; Okada, T.; Sakata, Y. *Angew. Chem. Int. Ed. Engl.* **1997**, *36*, 2626. (b) Luo, C.; Guldi, D. M.; Imahori, H.; Tamaki, K.; Sakata, Y. *J. Am. Chem. Soc.* **2000**, *122*, 6535. (c) Imahori, H.; Tamaki, K.; Guldi, D. M.; Luo, C.; Fujitsuka, M.; Ito, O.; Sakata, Y.; Fukuzumi, S. *J. Am. Chem. Soc.* **2001**, *123*, 2607. (d) Fukuzumi, S.; Imahori, H.; Yamada, H.; El-Khouly, M. E.; Fujitsuka, M.; Ito, O.; Guldi, D. M. *J. Am. Chem. Soc.* **2001**, *123*, 2571. (e) Imahori, H.; Guldi, D. M.; Tamaki, K.; Yoshida, Y.; Luo, C.; Sakata, Y.; Fukuzumi, S. *J. Am. Chem. Soc.* **2001**, *123*, 6617. (f) Imahori, H.; Tamaki, K.; Araki, Y.; Hasobe, T.; Ito, O.; Shimomura, A.; Kundu, S.; Okada, T.; Sakata, Y.; Fukuzumi, S. *J. Phys. Chem. A*, **2002**, *106*, 2803.

(23) (a) Imahori, H.; Yamada, H.; Nishimura, Y.; Yamazaki, I.; Sakata, Y. *J. Phys. Chem. B* **2000**, *104*, 2099. (b) Imahori, H.; Norieda, H.; Yamada, H.; Nishimura, Y.; Yamazaki, I.; Sakata, Y.; Fukuzumi, S. *J. Am. Chem. Soc.* **2001**, *123*, 100.

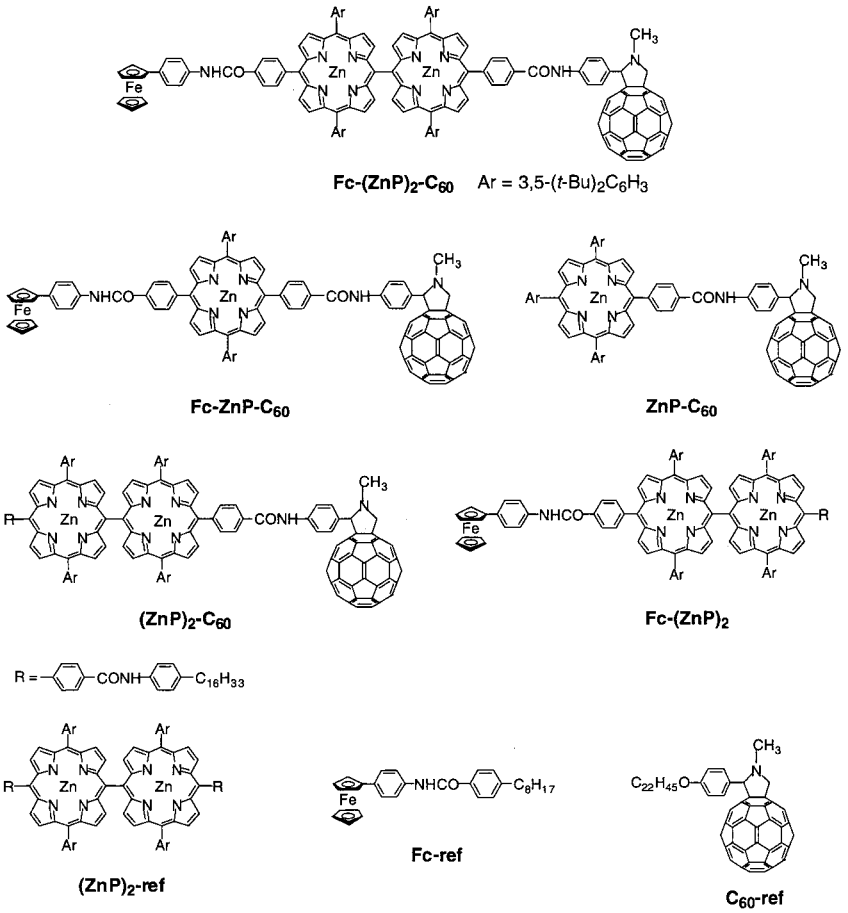

Figure 1. Ferrocene−porphyrin dimer−fullerene triad and the references used in this study.

$C_{60}^{\bullet-}$ radical ion pair (R_{ee} = 38.6 Å) by incorporating an additional porphyrin moiety. Thus, the lifetime of the final CS state is expected to be prolonged without lowering the charge separation efficiency when a similar stepwise ET occurs in Fc−$(ZnP)_2$−C_{60}. Although chemistry of *meso,meso*-linked porphyrin arrays has been developed rapidly,[24−27] ET studies on *meso,meso*-linked arrays with donor and acceptor units on the opposite ends have never been performed. Since the *meso,meso*-porphyrin arrays absorb visible light more widely than a linear combination of the corresponding porphyrin monomer as a result of the exciton coupling of the porphyrins,[24−27] the combination of *meso,meso*-porphyrin arrays with ferrocene as a donor and C_{60} as an acceptor is expected to enhance the light-harvesting capability. In the present study, the ET dynamics of Fc−$(ZnP)_2$−C_{60} have been investigated in full detail by time-resolved transient absorption spectroscopy and fluorescence lifetime measurements. We also report the temperature dependence for CR process from $C_{60}^{\bullet-}$ to Fc^+ in the final CS state, Fc^+−$(ZnP)_2$−$C_{60}^{\bullet-}$, which provides valuable insight into the important question as to why natural photosynthesis wastes a large fraction of the input energy to gain a long-lived CS state.

Results and Discussion

Synthesis. The preparation of Fc−$(ZnP)_2$−C_{60}, the reference dyads Fc−$(ZnP)_2$, $(ZnP)_2$−C_{60}, and the porphyrin reference $(ZnP)_2$-ref (Figure 1) was performed as shown in Schemes 1−3. *Trans*-AB_2C-type porphyrin **3** was prepared by the condensation of dipyrromethane **1**[28] and **2**[22b] with 3,5-di-*tert*-butylbenzaldehyde[29] in the presence of trifluoroacetic acid (TFA), followed by treatment with zinc acetate (Scheme 1). For the *meso,meso* coupling of **3**, we used the oxidant $AgPF_6$ in a mixture of chloroform and acetonitrile.[24] Because slight demetalation occurred under the present conditions, the crude mixture was treated with TFA and H_2SO_4 in chloroform to afford the freebase porphyrin, **4**. An important synthetic intermediate, **5**, was obtained by base hydrolysis of **4** in a mixture of THF and ethanol.

The freebase porphyrin carboxylic acid, **5**, was converted to the corresponding bis(acid chloride) **6** by treatment with $SOCl_2$ (Scheme 2). Cross-condensation of **6** with 4-aminophenylferrocene **7**[22c] and formyl-protected aniline **8**[30] in benzene in the presence of pyridine, followed by acid hydrolysis, afforded

(24) (a) Osuka, A.; Shimidzu, H. *Angew. Chem., Int. Ed. Engl.* **1997**, *36*, 135. (b) Tsuda, A.; Osuka, A. *Science* **2001**, *293*, 79.
(25) (a) Ohta, N.; Iwaki, Y.; Ito, T.; Yamazaki, I.; Osuka, A. *J. Phys. Chem. B* **1999**, *103*, 11242. (b) Piet, J. J.; Taylor, P. N.; Anderson, H. L.; Osuka, A.; Warman, J. M. *J. Am. Chem. Soc.* **2000**, *122*, 1749. (c) Kim, Y. H.; Jeong, D. H.; Kim, D.; Jeoung, S. C.; Cho, H. S.; Kim, S. K.; Aratani, N.; Osuka, A. *J. Am. Chem. Soc.* **2001**, *123*, 76.
(26) (a) Susumu, K.; Shimidzu, T.; Tanaka, K.; Segawa, H. *Tetrahedron Lett.* **1996**, *37*, 8399. (b) Khoury, R. G.; Jaquinod, L.; Smith, K. M. *Chem. Commun.* **1997**, 1057. (c) Vicente, M. G. H.; Jaquinod, L.; Smith, K. M. *Chem. Commun.* **1999**, 1771. (d) Miller, M. A.; Lammi, R. K.; Prathapan, S.; Holten, D.; Lindsey, J. S. *J. Org. Chem.* **2000**, *65*, 6634. (e) Clausen, C.; Gryko, D. T.; Yasseri, A. A.; Diers, J. R.; Bocian, D. F.; Kuhr, W. G.; Lindsey, J. S. *J. Org. Chem.* **2000**, *65*, 7371.
(27) Nakano, A.; Osuka, A.; Yamazaki, T.; Nishimura, Y.; Akimoto, S.; Yamazaki, I.; Itaya, A.; Murakami, M.; Miyasaka, H. *Chem. Eur. J.* **2001**, *7*, 3134.
(28) Wang, Q. M.; Bruce, D. W. *Synlett.* **1995**, 1267.
(29) Newman, M. S.; Lee, L. F. *J. Org. Chem.* **1972**, *37*, 4468.
(30) Imahori, H.; Azuma, T.; Ajavakom, A.; Norieda, H.; Yamada, H.; Sakata, Y. *J. Phys. Chem. B* **1999**, *103*, 7233.

Scheme 1

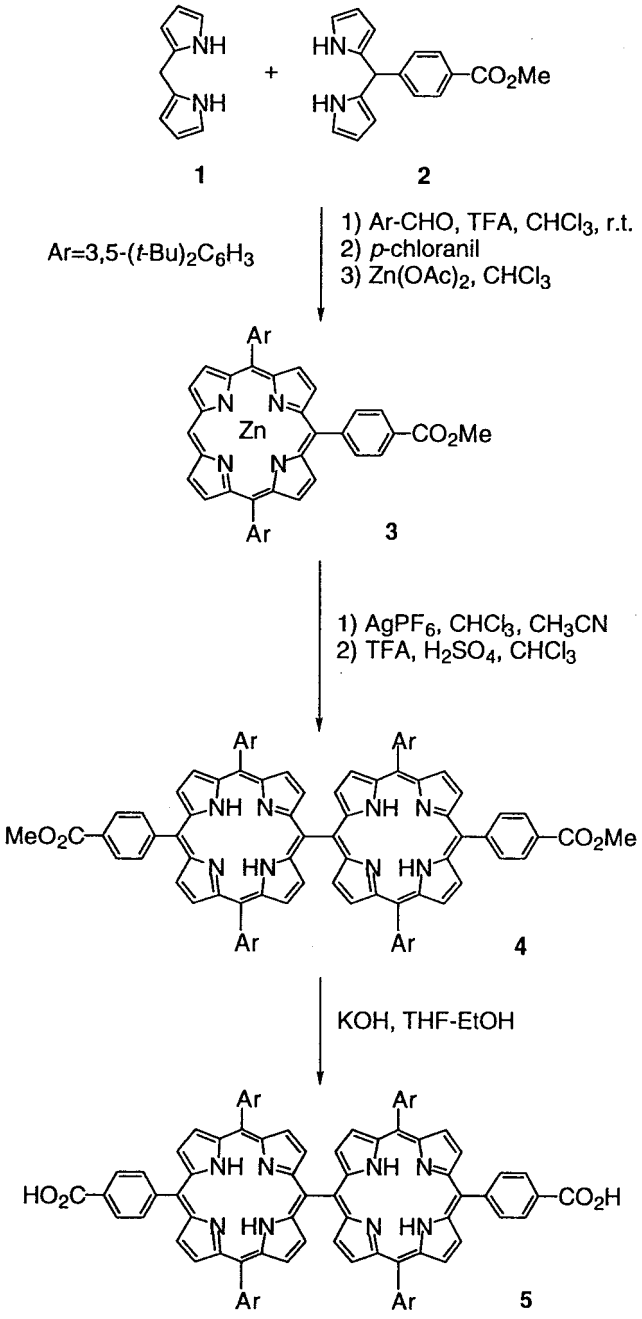

ferrocene-*meso*,*meso*-porphyrin dimer **9** in 20% yield. Fc−$(ZnP)_2$−C_{60} was obtained by 1,3-dipolar cycloaddition[31] using **9**, *N*-methylglycine and C_{60} in toluene and subsequent treatment with zinc acetate in 55% yield.

$(ZnP)_2$−C_{60} was synthesized from 4-hexadecylaniline, **6**, and **8**, via **10** by the same method as described for Fc−$(ZnP)_2$−C_{60} (Scheme 3). Fc−$(ZnP)_2$ and $(ZnP)_2$-ref were prepared from **7**, **6**, and 4-hexadecylaniline, and **6** and 4-hexadecylaniline, respectively. Single chromophore references Fc-ref[22c] and C_{60}-ref[22c] were also prepared by following the same procedures as described previously. Their structures were verified by spectroscopic analyses, including ^{1}H, FAB, and MALDI-TOF mass spectra (See Experimental Section).

(31) Maggini, M.; Scorrano, G.; Prato, M. *J. Am. Chem. Soc.* **1993**, *115*, 9798.

Absorption and Fluorescence Spectra. The absorption spectrum of Fc−$(ZnP)_2$−C_{60} in benzonitrile (PhCN) is virtually a linear combination of the spectra of Fc-ref, $(ZnP)_2$-ref, and C_{60}-ref (Figure 2). This indicates that there is no significant interaction among the three chromophores in the ground state. Similar superpositions of component spectra were found in THF and DMF. The absorption features of the porphyrin dimer in the visible region are much stronger than those of the ferrocene and the C_{60} moieties. It should be noted here that the sharp splitting of the Soret bands (∼430 and ∼470 nm) is characteristic of the *meso*,*meso*-linked porphyrins,[24−27] as seen in Figure 2. This enables us to harvest the light widely across the visible region, as compared to Fc−ZnP−C_{60} (inset of Figure 2).

Steady-state fluorescence spectra of Fc−$(ZnP)_2$−C_{60}, $(ZnP)_2$−C_{60}, and Fc−$(ZnP)_2$ in PhCN exhibit the same band shape and peak positions as that of $(ZnP)_2$-ref (λ_{em}^{max} = 637, 667 nm) when adjusting absorbance (0.25) at the excitation wavelength of 428 nm, where the porphyrin moiety absorbs light exclusively. No emission from the C_{60} (λ_{em}^{max} = 720 nm)[22] could be detected for Fc−$(ZnP)_2$−C_{60} and $(ZnP)_2$−C_{60}; however, fluorescence spectra of Fc−$(ZnP)_2$−C_{60} and $(ZnP)_2$−C_{60} in PhCN are quenched strongly as compared to those of $(ZnP)_2$-ref (relative intensities, 0.07 for Fc−$(ZnP)_2$−C_{60} and $(ZnP)_2$−C_{60}). In contrast, the relative fluorescence intensity of Fc−$(ZnP)_2$ versus $(ZnP)_2$-ref (0.55) in PhCN is much larger. Thus, quenching of the excited singlet porphyrin [$^1(ZnP)_2$*] by the attached C_{60} in Fc−$(ZnP)_2$−C_{60} is much faster than the quenching by the ferrocene (vide infra).

One-Electron Redox Potentials and ET Driving Force. The driving forces ($-\Delta G^0_{ET}$) for all the intramolecular ET processes were determined accurately by measuring the redox potentials of Fc−$(ZnP)_2$−C_{60} and the reference chromophores (Fc-ref, $(ZnP)_2$-ref, and C_{60}-ref) in various solvents. The differential pulse voltammetry was performed in THF, PhCN, and DMF solutions containing 0.1 M *n*-Bu_4NPF_6 as a supporting electrolyte. Although all of the compounds exhibited reversible redox waves in THF and PhCN, the poor solubility in DMF did not allow us to obtain reliable cyclic voltammograms under the same conditions. Table 1 summarizes all of the redox potentials of the investigated compounds. The redox potentials of Fc-ref and C_{60}-ref used as references were reported previously[22c] and are also summarized in Table 1. The first one-electron oxidation potentials (E^0_{ox}) of $(ZnP)_2$-ref (0.33 V vs ferrocene/ferricenium (Fc/Fc^+) and Fc-ref (−0.01 V vs Fc/Fc^+) and the first one-electron reduction potentials (E^0_{red}) of C_{60}-ref (−1.04 V vs Fc/Fc^+) and $(ZnP)_2$-ref (−1.79 V vs Fc/Fc^+) in PhCN are virtually the same as those of Fc−$(ZnP)_2$−C_{60} (0.34, 0.00, −1.05, −1.81 V vs Fc/Fc^+, respectively) in PhCN. This implies that electronic interactions among the ferrocene, the porphyrin dimer, and the C_{60} are negligible in the ground state. $(ZnP)_2$-ref exhibits negative shifts for the first one-electron oxidation potentials with increasing solvent polarity. Positive shifts were noted for the first one-electron reduction potentials of C_{60}-ref[22c] and $(ZnP)_2$-ref. On the other hand, the first one-electron oxidation potential of Fc-ref remains nearly constant, despite the substantial increase in solvent polarity.[22c]

The driving forces ($-\Delta G^0_{ET(CR)}$ in eV) for the intramolecular CR processes from the C_{60} radical anion ($C_{60}^{\bullet-}$) to the zinc porphyrin dimer radical cation [$(ZnP)_2^{\bullet+}$] or the ferricenium ion

Scheme 2

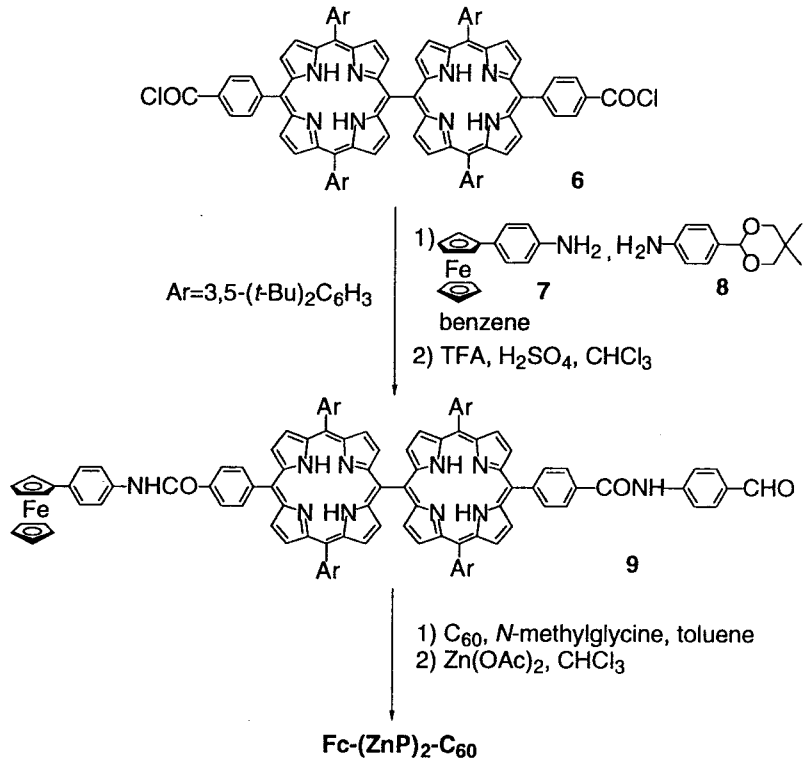

Scheme 3

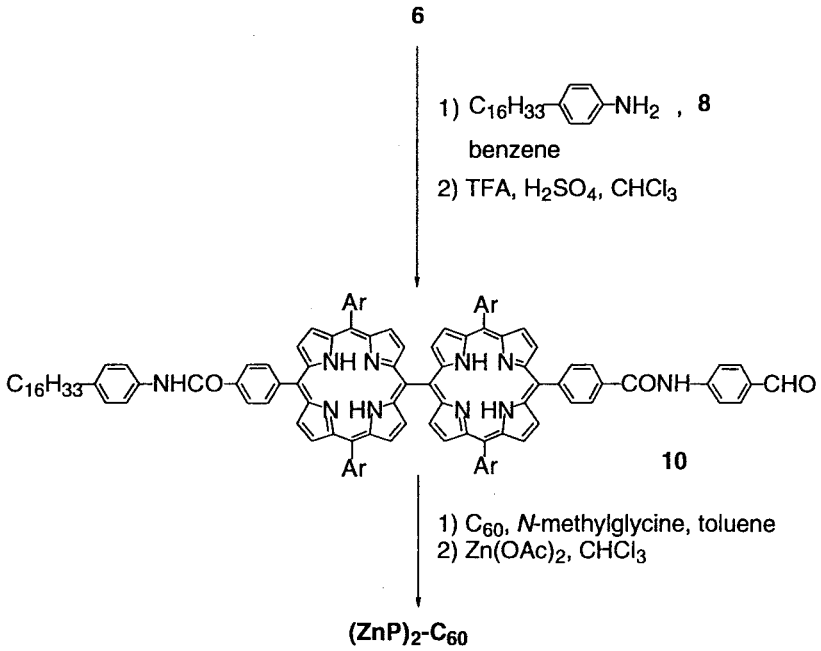

(Fc^+) in Fc−$(ZnP)_2$−C_{60} and $(ZnP)_2$−C_{60} were determined by eq 1, where *e* stands for the elementary charge. The $-\Delta G^0_{ET(CR)}$ values (in eV), thus obtained in THF, PhCN, and DMF, are listed in Tables 2 and 3.

$$-\Delta G^0_{ET(CR)} = e[E^0_{ox}(D^{\bullet+}/D) - E^0_{red}(A/A^{\bullet-})] \quad (1)$$

The driving forces for the intramolecular charge separation processes ($-\Delta G^0_{ET(CS)}$ in eV) from the porphyrin dimer singlet excited state to the C_{60} in Fc−$(ZnP)_2$−C_{60} and $(ZnP)_2$−C_{60} were determined by eq 2, where ΔE_{0-0} is the energy of the 0−0 transition energy gap between the lowest excited state and the ground state, which is determined by the 0−0* absorption and 0*−0 fluorescence maxima in solvents (* denotes the excited state). The $-\Delta G^0_{ET(CS)}$ values are given in Tables 2 and 3. The driving forces for intramolecular charge-shift (CSH) processes ($-\Delta G^0_{ET(CSH)}$ in eV) from the Fc to the $(ZnP)_2^{\bullet+}$ in Fc−$(ZnP)_2$−C_{60} were determined by subtracting the energy of the final state from that of the initial state (Table 3). It should be noted that

$$-\Delta G^0_{ET(CS)} = \Delta E_{0-0} + \Delta G^0_{ET(CR)} \quad (2)$$

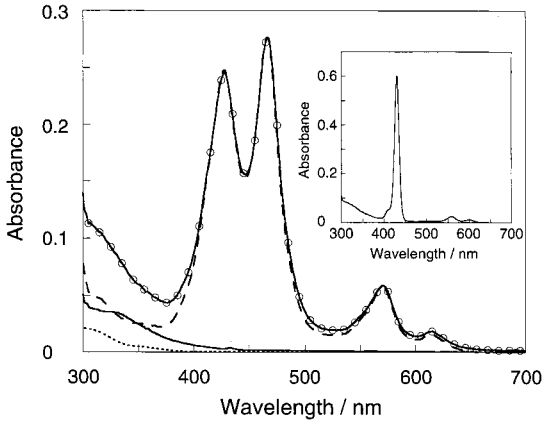

Figure 2. Absorption spectra of Fc−$(ZnP)_2$−C_{60} (solid line with circles), Fe-ref (dotted line), $(ZnP)_2$-ref (dashed line), and C_{60}-ref (solid line) in PhCN (1.0×10^{-6} M). Absorption spectrum of Fc−ZnP−C_{60} in PhCN (1.0×10^{-6} M) is depicted in the inset.

Table 1. One-Electron Redox Potentials (vs Fc/Fc^+)[a] of Triad and the References in Various Solvents

		E^0_{ox}/V		E^0_{red}/V	E^0_{red}/V
compound	solvent	$(ZnP)_2^{\bullet+}/(ZnP)_2$	Fc^+/Fc	$C_{60}/C_{60}^{\bullet-}$	$(ZnP)_2/(ZnP)_2^{\bullet-}$
Fc−$(ZnP)_2$−C_{60}	PhCN	0.34	0.00	−1.05	−1.81
$(ZnP)_2$-ref	PhCN	0.33			−1.79
Fc-ref			−0.01[b]		
C_{60}-ref				−1.04[b]	
$(ZnP)_2$-ref	THF	0.38			−1.91
Fc-ref			−0.02[b]		
C_{60}-ref				−1.02[b]	
$(ZnP)_2$-ref	DMF	0.27			−1.75
Fc-ref			−0.01[b]		
C_{60}-ref				−0.92[b]	

[a] The redox potentials were measured by differential pulse voltammetry in THF, PhCN, and DMF using 0.1 M *n*-Bu_4NPF_6 as a supporting electrolyte with a sweep rate of 10 mV s^{-1}. [b] From ref 22c.

the Coulombic terms in the present donor−acceptor systems are largely neglected in the evaluation of the driving forces in Tables 2 and 3, especially in solvents with moderate or high polarity, because of the relatively long edge-to-edge distance (R_{ee} > 11 Å) employed.[22c]

Photodynamics of Porphyrin-Fullerene-Linked Systems. Time-resolved transient absorption spectra, following picosecond and nanosecond laser pulses, were employed to examine the photodynamics of $(ZnP)_2$-ref, $(ZnP)_2$−C_{60}, Fc−$(ZnP)_2$, and Fc−$(ZnP)_2$−C_{60}. To monitor the intramolecular ET dynamics, the absorption of the one-electron-reduced form of the electron acceptor ($C_{60}^{\bullet-}$) was analyzed in the near-infrared region (NIR) around 1000 nm.

$(ZnP)_2$-ref. Nano- and picosecond time-resolved transient absorptions of $(ZnP)_2$-ref in PhCN are displayed in Figure 3a and Figure 4, respectively. Picosecond excitation (388 nm) of $(ZnP)_2$-ref resulted in characteristic absorption changes in the 450−750 nm and 800−1100 nm range, as shown in Figure 4 (dotted line). In particular, a net decrease of the absorption was observed around 580 and 620 nm, which is dominated by the strong ground-state absorption. This suggests that the porphyrin singlet ground state is converted to the corresponding singlet excited state [$^1(ZnP)_2$*].[32] $^1(ZnP)_2$* also exhibits a strong absorption band at 505 nm. Intersystem crossing is the predominant fate of the singlet excited state. The resultant triplet excited state [$^3(ZnP)_2$*][32] reveals a characteristic peak around 840 nm (Figure 3a), whereas no characteristic absorption around 800−1000 nm appears in the picosecond absorption spectrum (Figure 4).

The porphyrin radical cation [$(ZnP)_2^{\bullet+}$][33] produced by the chemical oxidation of $(ZnP)_2$-ref with $Fe(bpy)_3^{3+}$ (bpy = 2,2′-bipyridine)[34] exhibits broad absorption around 500−1000 nm, as shown in Figure 3b. The absorption coefficient at 646 nm in PhCN was determined to be 10700 M^{-1} cm^{-1}. In summary, the above features of $^1(ZnP)_2$*, $^3(ZnP)_2$*, and $(ZnP)_2^{\bullet+}$ are easily detectable markers for the following intramolecular ET reactions.

$(ZnP)_2$−C_{60}. Time-resolved transient absorption spectra of $(ZnP)_2$−C_{60} were also measured by pico- and nanosecond laser photolysis. Picosecond time-resolved absorption spectrum of $(ZnP)_2$−C_{60} in PhCN is shown in Figure 4. $(ZnP)_2$−C_{60} was excited at 388 nm, where the porphyrin moiety absorbs light mainly. The differential spectrum taken immediately after the laser pulse is characterized by the bleaching of the porphyrin Q-band absorption at 580 and 620 nm due to the $^1(ZnP)_2$*. As time delays, a new transition around 1000 nm grows in, accompanied by another broad absorption around 650 nm (solid line in Figure 4), which is quite different from the spectral features of $^1(ZnP)_2$* and $^3(ZnP)_2$*. By comparison with the absorption of $C_{60}^{\bullet-}$ and $(ZnP)_2^{\bullet+}$ (vide supra),[21,22] we ascribe the former and the latter bands to the $C_{60}^{\bullet-}$ moiety[35] and the $(ZnP)_2^{\bullet+}$ moiety, respectively. This indicates the occurrence of a photoinduced ET, evolving from $^1(ZnP)_2$* to the C_{60} and, in turn, creating the $(ZnP)_2^{\bullet+}$−$C_{60}^{\bullet-}$ state. The energy levels in PhCN, as extracted from Table 2, are shown in Scheme 4 to illustrate the relaxation pathways of photoexcited $(ZnP)_2$−C_{60}. Similar transient absorption spectra, specifically, the spectral fingerprints of $(ZnP)_2^{\bullet+}$ and $C_{60}^{\bullet-}$, were obtained in THF and DMF.

The fluorescence lifetimes (τ) of $(ZnP)_2$−C_{60} and $(ZnP)_2$-ref were also measured with a time-correlated single-photon-counting apparatus by using a 410-nm excitation where the

Table 2. ET Rate Constants (k_{ET}), Quantum Yields (Φ) and the Driving Forces ($-\Delta G^0_{ET}$) in $(ZnP)_2$−C_{60}

solvent	initial state[a]	final state[a]	$-\Delta G^0_{ET}$/eV	k_{ET}/s^{-1}[b]	Φ[c]
PhCN	$^1(ZnP)_2$*−C_{60} (2.00 eV)	$(ZnP)_2^{\bullet+}$−$C_{60}^{\bullet-}$ (1.37 eV)	0.63	$k_{ET(CS1)} = 6.6 \times 10^9$	$\Phi_{CS1}(^1ZnP^*) = 0.93$
(ϵ_s = 25.2)	$(ZnP)_2^{\bullet+}$−$C_{60}^{\bullet-}$ (1.37 eV)	$(ZnP)_2$−C_{60}	1.37	$k_{ET(CR1)} = 1.9 \times 10^6$	
THF	$^1(ZnP)_2$*−C_{60} (2.02 eV)	$(ZnP)_2^{\bullet+}$−$C_{60}^{\bullet-}$ (1.40 eV)	0.62	$k_{ET(CS1)} = 7.1 \times 10^9$	$\Phi_{CS1}(^1ZnP^*) = 0.92$
(ϵ_s = 7.58)	$(ZnP)_2^{\bullet+}$−$C_{60}^{\bullet-}$ (1.40 eV)	$(ZnP)_2$−C_{60}	1.40	$k_{ET(CR1)} = 1.0 \times 10^6$	
DMF	$^1(ZnP)_2$*−C_{60} (2.00 eV)	$(ZnP)_2^{\bullet+}$−$C_{60}^{\bullet-}$ (1.19 eV)	0.81	$k_{ET(CS1)} = 4.7 \times 10^9$	$\Phi_{CS1}(^1ZnP^*) = 0.89$
(ϵ_s = 36.7)	$(ZnP)_2^{\bullet+}$−$C_{60}^{\bullet-}$ (1.19 eV)	$(ZnP)_2$−C_{60}	1.19	$k_{ET(CR1)} = 3.4 \times 10^6$	

[a] The energy of each state relative to the ground state is given in parentheses. [b] The k_{ET} values for ET from $^1(ZnP)_2$* to C_{60} were determined from the fluorescence lifetimes by using the equation, $k_{ET} = [1/\tau((ZnP)_2-C_{60})] - [1/\tau((ZnP)_2\text{-ref})]$. The k_{ET} values for CR were determined by analyzing the decay of $C_{60}^{\bullet-}$ at 1000 nm. [c] The efficiency (Φ) for charge separation was estimated on the basis of Scheme 4.

Table 3. ET Rate Constants (k_{ET}), Quantum Yields (Φ) and the Driving Forces ($-\Delta G^0_{ET}$) in Fc-$(ZnP)_2$-C_{60}

solvent	initial state[a]	final state[a]	$-\Delta G^0_{ET}$/eV	k_{ET}/ s^{-1}[b]	Φ[c]
PhCN	Fc−$^1(ZnP)_2$*−C_{60} (2.00 eV)	Fc−$(ZnP)_2^{\bullet+}$−$C_{60}^{\bullet-}$ (1.37 eV)	0.63	$k_{ET(CS1)} = 5.0 \times 10^9$	$\Phi_{CS1}(^1ZnP^*) = 0.85$
	Fc−$^1(ZnP)_2$*−C_{60} (2.02 eV)	Fc^+−$(ZnP)_2^{\bullet-}$−C_{60} (1.78 eV)	0.24	$k_{ET(CS2)} = 3.5 \times 10^8$	$\Phi_{CS2}(^1ZnP^*) = 0.06$
($\epsilon_s = 25.2$)	Fc−$(ZnP)_2^{\bullet+}$−$C_{60}^{\bullet-}$ (1.37 eV)	Fc^+−$(ZnP)_2$−$C_{60}^{\bullet-}$ (1.03 eV)	0.34	$k_{ET(CSH1)} = 1.3 \times 10^7$	$\Phi_{CSH1} = 0.87$
	Fc^+−$(ZnP)_2$−$C_{60}^{\bullet-}$ (1.03 eV)	Fc−$(ZnP)_2$−C_{60}	1.03	$k_{ET(CR)obs} = 5.3 \times 10^4$[d]	Φ_{CS}(total) = 0.80
THF	Fc−$^1(ZnP)_2$*−C_{60} (2.02 eV)	Fc−$(ZnP)_2^{\bullet+}$−$C_{60}^{\bullet-}$ (1.40 eV)	0.62	$k_{ET(CS1)} = 3.3 \times 10^9$	$\Phi_{CS1}(^1ZnP^*) = 0.83$
	Fc−$^1(ZnP)_2$*−C_{60} (2.02 eV)	Fc^+−$(ZnP)_2^{\bullet-}$−C_{60} (1.89 eV)	0.13	$k_{ET(CS2)} = 1.6 \times 10^8$	$\Phi_{CS2}(^1ZnP^*) = 0.04$
($\epsilon_s = 7.58$)	Fc−$(ZnP)_2^{\bullet+}$−$C_{60}^{\bullet-}$ (1.40 eV)	Fc^+−$(ZnP)_2$−$C_{60}^{\bullet-}$ (1.00 eV)	0.40	$k_{ET(CSH1)} = 4.2 \times 10^6$	$\Phi_{CSH1} = 0.81$
	Fc^+−$(ZnP)_2$−$C_{60}^{\bullet-}$ (1.00 eV)	Fc−$(ZnP)_2$−C_{60}	1.00	$k_{ET(CR)obs} = 6.3 \times 10^4$[d]	Φ_{CS}(total) = 0.71
DMF	Fc−$^1(ZnP)_2$*−C_{60} (2.00 eV)	Fc−$(ZnP)_2^{\bullet+}$−$C_{60}^{\bullet-}$ (1.19 eV)	0.81	$k_{ET(CS1)} = 1.1 \times 10^{10}$	$\Phi_{CS1}(^1ZnP^*) = 0.92$
	Fc−$^1(ZnP)_2$*−C_{60} (2.02 eV)	Fc^+−$(ZnP)_2^{\bullet-}$−C_{60} (1.74 eV)	0.28	$k_{ET(CS2)} = 4.1 \times 10^8$	$\Phi_{CS2}(^1ZnP^*) = 0.03$
($\epsilon_s = 36.7$)	Fc−$(ZnP)_2^{\bullet+}$−$C_{60}^{\bullet-}$ (1.19 eV)	Fc^+−$(ZnP)_2$−$C_{60}^{\bullet-}$ (0.91 eV)	0.28	$k_{ET(CSH1)} = 3.3 \times 10^7$	$\Phi_{CSH1} = 0.92$
	Fc^+−$(ZnP)_2$−$C_{60}^{\bullet-}$ (0.91 eV)	Fc−$(ZnP)_2$−C_{60}	0.91	$k_{ET(CR)obs} = 1.2 \times 10^4$[d]	Φ_{CS}(total) = 0.88

[a] The energy of each state relative to the ground state is given in parentheses. [b] The $k_{ET(CS)}$ values for ET from $^1(ZnP)_2$* to C_{60} and Fc to $^1(ZnP)_2$* were determined from the fluorescence lifetimes by using the equations, $k_{ET(CS1)} = [1/\tau\ (Fc{-}(ZnP)_2{-}C_{60})] - [1/\tau\ (Fc{-}(ZnP)_2)]$ and $k_{ET(CS2)} = [1/\tau\ (Fc{-}(ZnP)_2)] - [1/\tau\ ((ZnP)_2\text{-ref})]$. The $k_{ET(CSH1)}$ values were determined from the decay rate constants of $(ZnP)_2^{\bullet+}$ for Fc−$(ZnP)_2$−C_{60} in reference to those of $(ZnP)_2$−C_{60}. The $k_{ET(CR)obs}$ values were determined by analyzing the decay of $C_{60}^{\bullet-}$ at 1000 nm. [c] The efficiencies (Φ) for each deactivation pathway were estimated on the basis of Scheme 5. [d] At 295 K.

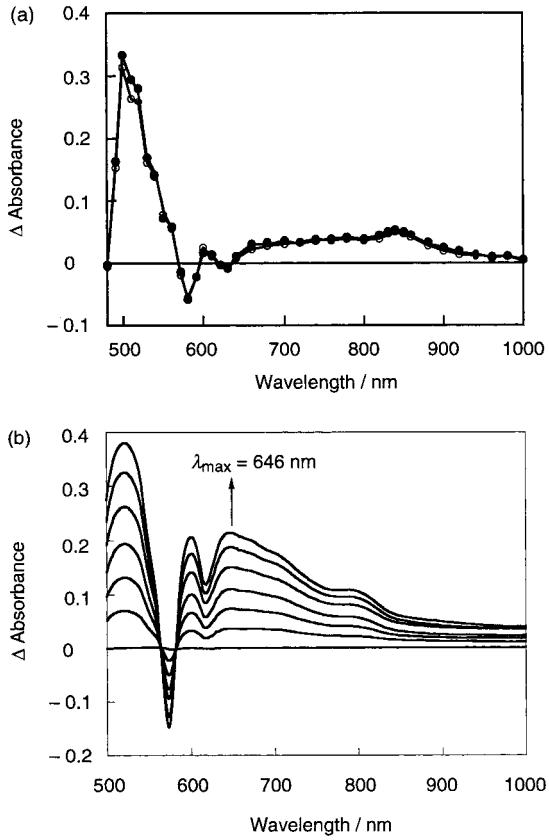

Figure 3. (a) Differential absorption spectra obtained upon nanosecond flash photolysis (530 nm) of 0.1 mM solution of $(ZnP)_2$-ref in argon-saturated PhCN with a time delay of 100 ns (solid circles) and 1000 ns (open circles). (b) Spectral change in the addition of $Fe(bpy)_3^{3+}$ (0.17, 0.33, 0.50, 0.67, 0.83, and 1.0 eqiv) in deaerated PhCN solution containing $(ZnP)_2$-ref (2.0×10^{-5} M).

porphyrin moiety absorbs light exclusively. The fluorescence decay was monitored at 630 nm, relating to the emission of only the porphyrin moiety. No emission from the C_{60} moiety was detected for $(ZnP)_2$−C_{60}, even at 720 nm.[22] In general, the fluorescence decay curves were well-fitted by a single-exponential decay component. The fluorescence lifetimes are listed in Table 4. On the basis of the fluorescence lifetimes (λ_{obs} = 630 nm) in PhCN, the ET rate constants were determined as

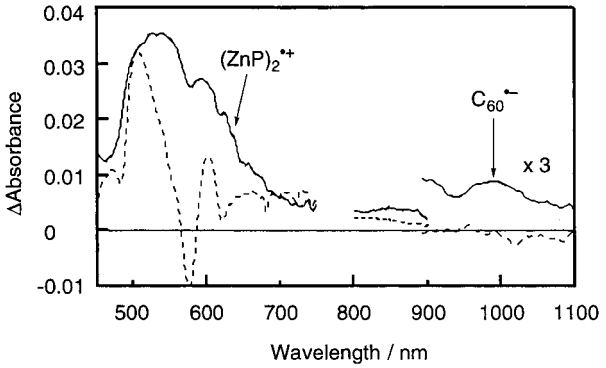

Figure 4. Picosecond time-resolved absorption spectra of $(ZnP)_2$-ref (dotted line) and $(ZnP)_2$−C_{60} (solid line) at a time delay of 1000 ps excited at 388 nm in argon-saturated PhCN. The spectrum of $(ZnP)_2$-ref is normalized at 505 nm for comparison.

Scheme 4. Reaction Scheme and Energy Diagram for $(ZnP)_2$−C_{60} in PhCN

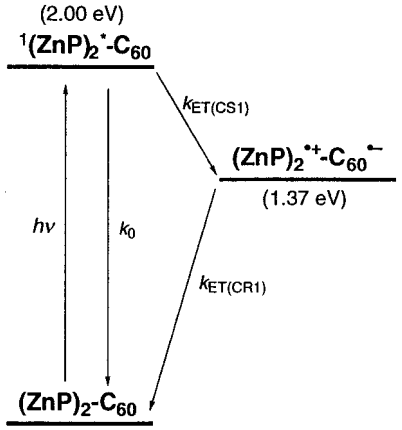

$k_{ET(CS1)} = 6.6 \times 10^9\ s^{-1}$ for ET from ^{1}ZnP* to C_{60} with the quantum efficiency of $\Phi_{CS1}(^1ZnP^*) = k_{ET(CS1)}/(k_{ET(CS1)} + k_0) = 0.93$. Similar $k_{ET(CS1)}$ values were also determined as 7.1 ×

(32) Exciton delocalization in singlet and triplet excited states was reported in similar *meso, meso*-linked zincporphyrin arrays.[25b, c]

(33) The absorption spectrum of $(ZnP)_2^{\bullet+}$ is similar to that of zinc *meso*-tetraphenylporphyrin.[22] Although the two porphyrins are directly linked at the meso positions where the electron density of the radical cation is large relative to the other positions, the two porphyrin planes are orthogonal due to the steric hindrance.[24−27] Thus, the charge delocalization onto both the porphyrins may be relatively small. However, the degree of charge delocalization has yet to be clarified.

(34) Fukuzumi, S.; Miyamoto, K.; Suenobu, T.; Van Caemelbecke, E.; Kadish, K. M. *J. Am. Chem. Soc.* **1998**, *120*, 2880.
(35) Guldi, D. M.; Hungerbühler, H.; Asmus, K.-D. *J. Phys. Chem.* **1995**, *99*, 9380.

Table 4. Fluorescence Lifetimes of $(ZnP)_2-C_{60}$, $Fc-(ZnP)_2-C_{60}$, and the Reference Compounds in THF, PhCN, and DMF[a]

	fluorescence lifetime (τ) (ps)		
compd	PhCN ($\epsilon_s = 25.2$)	THF ($\epsilon_s = 7.58$)	DMF ($\epsilon_s = 36.7$)
$(ZnP)_2-C_{60}$	140	130	190
$(ZnP)_2$-ref	1800	1800	2000
$Fc-(ZnP)_2-C_{60}$	170	250	81
$Fc-(ZnP)_2$	1100	1400	1100

[a] Excitation wavelength, 410 nm; monitoring wavelength, 630 nm.

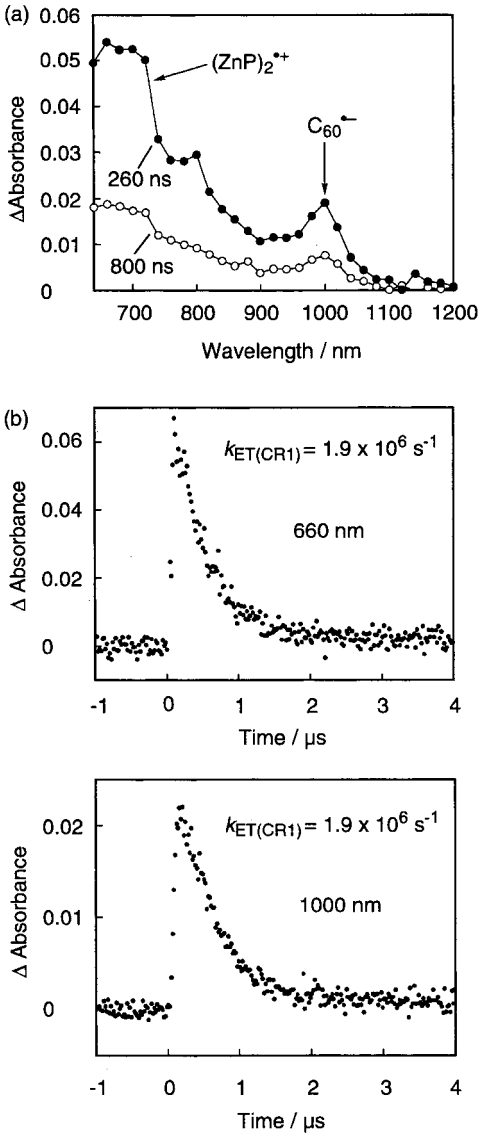

Figure 5. (a) Nanosecond time-resolved absorption spectra of $(ZnP)_2-C_{60}$ (0.1 mM) in argon-saturated PhCN excited at 530 nm. The delay times between the excitation and the measurement are indicated on the left. (b) The time profiles of absorbance at 660 and 1000 nm at 295 K.

10^9 s^{-1} in THF and 4.7×10^9 s^{-1} in DMF (Table 2). These results are similar to those of the corresponding reference, $ZnP-C_{60}$ in Figure 1.[21c,22c]

Formation of $C_{60}^{\bullet-}$ (1000 nm) and $(ZnP)_2^{\bullet+}$ (broad absorption around 650 nm) was further substantiated (Figure 5) by a set of complementary nanosecond experiments by using a 530-nm excitation where the porphyrin moiety absorbs light exclusively. The transient absorption spectrum obtained from $(ZnP)_2-C_{60}$ in Figure 5 matches well the spectrum in Figure 4, corroborating

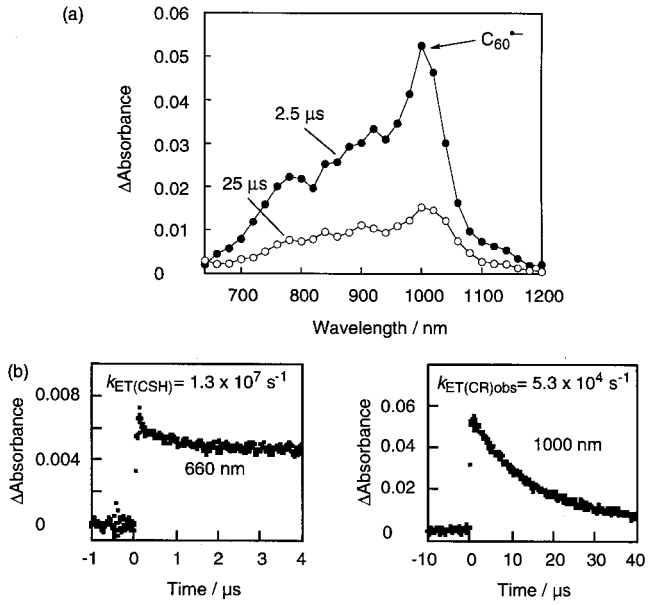

Figure 6. (a) Nanosecond time-resolved absorption spectra of $Fc-(ZnP)_2-C_{60}$ (0.1 mM) in argon-saturated PhCN excited at 530 nm. The delay times between the excitation and the measurement are indicated on the left. (b) The time profiles of absorbance at 660 and 1000 nm at 295 K.

Scheme 5. Reaction Scheme and Energy Diagram for $Fc-(ZnP)_2-C_{60}$ in PhCN

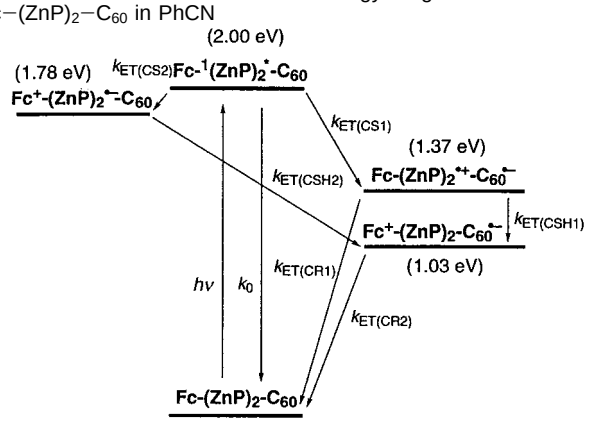

the formation of $C_{60}^{\bullet-}$ and $(ZnP)_2^{\bullet+}$. The resulting CS state recombines to regenerate the singlet ground state. From the decay kinetics at 1000 and 660 nm, a rate constant ($k_{ET(CR1)}$) of 1.9×10^6 s^{-1} is deduced for a PhCN solution. This rate constant is virtually the same as that of the corresponding reference, $ZnP-C_{60}$, in Figure 1 ($k_{ET(CR1)} = 1.3 \times 10^6$ s^{-1}).[21c,22c]

The photodynamic behavior of the $(ZnP)_2-C_{60}$ in THF and DMF is similar to that described in PhCN (Table 2). A possible explanation for this analogy is based on the corresponding energy levels. In particular, the energies of the excited states (i.e., $^1(ZnP)_2$* (2.00−2.02 eV), $^3(ZnP)_2$* (1.55 eV), $^1C_{60}$* (1.75 eV), and $^3C_{60}$* (1.50 eV)) are substantially higher than the energy of the CS state in THF (1.40 eV), PhCN (1.37 eV), and DMF (1.19 eV). This, in turn, guarantees large driving forces for the associated charge separation and CR processes.

$Fc-(ZnP)_2-C_{60}$. The energy levels in PhCN, which are expected to be of significance for the photoinduced ET reactions in $Fc-(ZnP)_2-C_{60}$, are taken from the data summarized in Table 3, and they are diagrammed in Scheme 5.

Picosecond-time-resolved absorption spectra of $Fc-(ZnP)_2-C_{60}$ after a laser pulse (388 nm) were taken in PhCN. The

spectral behavior of Fc−$(ZnP)_2$−C_{60} is similar to that of $(ZnP)_2$−C_{60} (Figure 4). This clearly shows that photoinduced ET occurs from the $^1(ZnP)_2$* to the C_{60} moiety to generate Fc−$(ZnP)_2^{\bullet+}$−$C_{60}^{\bullet-}$. The rate constant ($k_{ET(CS1)} = 5.0 \times 10^9$ s^{-1}) and the efficiency of formation of Fc−$(ZnP)_2^{\bullet+}$−$C_{60}^{\bullet-}$ from $^1(ZnP)_2$* ($\Phi_{CS1}(^1ZnP^*) = 0.85$) were determined as described for $(ZnP)_2$−C_{60} (Table 3). The fluorescence lifetime of Fc−$(ZnP)_2$ indicates that photoinduced ET also occurs from Fc to $^1(ZnP)_2$* to produce Fc^+−$(ZnP)_2^{\bullet-}$ (Table 4). However, the ET from Fc to $^1(ZnP)_2$* ($k_{ET(CS2)} = 3.5 \times 10^8$ s^{-1}) is much slower, by a factor of 1/14, than the ET from $^1(ZnP)_2$* to C_{60}. Thus, the deactivation pathway to generate Fc^+−$ZnP^{\bullet-}$−C_{60} is rather negligible, although the CS state would undergo CSH ($-\Delta G^0_{ET(CSH2)} = 0.75$ eV) to the C_{60} moiety to generate Fc^+−$(ZnP)_2$−$C_{60}^{\bullet-}$ efficiently.

Nanosecond transient-absorption spectra of Fc−$(ZnP)_2$−C_{60} at a time delay of 2.5−25 μs also exhibit formation of $C_{60}^{\bullet-}$ around 1000 nm, whereas the transient absorption due to the $(ZnP)_2^{\bullet+}$ around 660 nm disappears (Figure 6a), in contrast with the case of $(ZnP)_2$−C_{60} (Figure 5a). The absorption spectrum is virtually identical to that of Fc^+−ZnP−$C_{60}^{\bullet-}$.[22c] Taking into account the small molar absorption coefficient of the ferricenium ion ($\epsilon \sim 1000$ M^{-1} cm^{-1} at 800 nm),[22c] it is concluded that the resulting CS state (Fc−$(ZnP)_2^{\bullet+}$−$C_{60}^{\bullet-}$) undergoes the CSH from the Fc moiety to generate Fc^+−$(ZnP)_2$−$C_{60}^{\bullet-}$. In fact, the time profile of absorption around 660 nm can be fitted by a fast decay [$\tau((ZnP)_2^{\bullet+}) = 67$ ns] (Figure 6b), which corresponds to the CSH from the Fc moiety to the $(ZnP)_2^{\bullet+}$ ($k_{ET(CSH1)} = 1.3 \times 10^7$ s^{-1}).[36] The CSH value is smaller by 2 orders of magnitude than that of Fc−ZnP−C_{60} (2.8×10^9 s^{-1}).[22c,37] Given that the $k_{ET(CR1)}$ value of Fc−$(ZnP)_2^{\bullet+}$−$C_{60}^{\bullet-}$ is the same as that of $(ZnP)_2^{\bullet+}$−$C_{60}^{\bullet-}$ (1.9×10^6 s^{-1}), the quantum yield of CSH (Φ_{CSH1}) is found to be 0.87, according to eq 3.

$$\Phi_{CSH1} = \frac{k_{ET(CSH1)}}{k_{ET(CR1)} + k_{ET(CSH1)}} \qquad (3)$$

Assuming that the quantum yield of CSH from Fc^+−$(ZnP)_2^{\bullet-}$−C_{60} to Fc^+−$(ZnP)_2$−$C_{60}^{\bullet-}$ is unity ($\Phi_{CSH2} = 1$), the overall quantum yield of the formation of Fc^+−$(ZnP)_2$−$C_{60}^{\bullet-}$ [$\Phi_{CS}(\text{total}) = \Phi_{CS1}\Phi_{CSH1} + \Phi_{CS2}\Phi_{CSH2}$] is determined as 0.80 (Table 3). Similar photodynamical behavior was observed in THF ($\Phi_{CS}(\text{total}) = 0.71$) and DMF ($\Phi_{CS}(\text{total}) = 0.88$), and the results are summarized in Table 3.[38] The overall quantum yields of the formation of Fc^+−$(ZnP)_2$−$C_{60}^{\bullet-}$ are as large as those of Fc^+−ZnP−$C_{60}^{\bullet-}$, despite of the larger R_{ee} value in the former.

Stepwise CR Processes. The CR rate constants ($k_{ET(CR)obs}$) of the CS states (i.e., Fc^+−$(ZnP)_2$−$C_{60}^{\bullet-}$) at 295 K have been determined by analyzing the decay kinetics of the $C_{60}^{\bullet-}$ moiety in various polar solvents, and the results are also summarized in Table 3. The time-absorption profiles were fitted as a single-exponential decay. The CR rate constants of Fc^+−$(ZnP)_2$−$C_{60}^{\bullet-}$ (6.3×10^4 s^{-1} (THF), 5.3×10^4 s^{-1} (PhCN), and 1.2×10^4 s^{-1} (DMF)) decrease with increasing solvent polarity. Interestingly, they are smaller than those of Fc^+−ZnP−$C_{60}^{\bullet-}$ (2.7×10^5 s^{-1} (THF); 1.3×10^5 s^{-1} (PhCN); 6.3×10^4 s^{-1} (DMF))[22c] by only a factor of ~1/4−1/2, despite the significant increase of the R_{ee} values ($\Delta R_{ee} = 8.3$ Å).[22c] We reported the distance dependence of an electronic coupling matrix element in a homologous series of porphyrin-fullerene dyad and triad (i.e., ZnP−C_{60}, Fc−ZnP−C_{60}), and the damping factor (β) was determined to be 0.58 $Å^{-1}$.[22c] Given the β value together with the λ value (~1.2 eV),[22c] the CR rate constant from $C_{60}^{\bullet-}$ to Fc^+ ($k_{ET(CR2)}$) is anticipated to be ~10^2 s^{-1}, which is 2 orders of magnitude smaller than the experimental values.

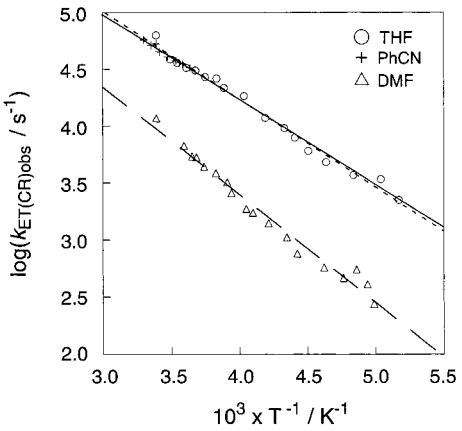

Figure 7. Arrhenius plots of the CR rate for Fc^+−$(ZnP)_2$−$C_{60}^{\bullet-}$ [log($k_{ET(CR)obs}$)] in THF (circle), PhCN (cross), and DMF (triangle).

To clarify the reason for this discrepancy between the observed and the expected CR rates, the temperature dependence of the intramolecular CR rates in the triads was examined in THF, PhCN, and DMF. The Arrhenius plots, the logarithmic CR rate of Fc^+−$(ZnP)_2$−$C_{60}^{\bullet-}$ [log($k_{ET(CR)obs}$)] vs T^{-1}, reveal no appreciable deviation from the best-fitted straight line (Figure 7). From the observed temperature dependence, the activation energies (E_a) were determined to be 0.16 eV in THF, 0.15 eV in PhCN, and 0.19 eV in DMF.

The appreciable activation energies observed for the CR processes contradict the fact that the CR processes (the driving force is in the range of 0.91−1.03 eV in Table 3) are nearly on the top region of the Marcus parabola, when the activation energies of the direct CR processes would be close to zero. The observed E_a values (0.15−0.19 eV) are rather comparable to the energy difference between Fc^+−$(ZnP)_2$−$C_{60}^{\bullet-}$ and Fc−$(ZnP)_2^{\bullet+}$−$C_{60}^{\bullet-}$ (0.34 eV in PhCN), the value of which was evaluated by neglecting the Coulombic interaction in the radical ion pair (vide supra). The smaller E_a values, as compared to the energy difference, may be ascribed to the difference in the Coulombic term, which should be larger in Fc−$(ZnP)_2^{\bullet+}$−$C_{60}^{\bullet-}$ than in Fc^+−$(ZnP)_2$−$C_{60}^{\bullet-}$ because of the larger edge-to-edge distance in the latter.[39] Thus, the back ET to the ground state occurs via the reversed stepwise processes, that is, a rate-limiting ET from $(ZnP)_2$ to Fc^+ to give the initial CS state (Fc−$(ZnP)_2^{\bullet+}$−$C_{60}^{\bullet-}$), followed by a fast ET from $C_{60}^{\bullet-}$ to $(ZnP)_2^{\bullet+}$ to regenerate the ground state, Fc−$(ZnP)_2$−C_{60}.[40]

It is intriguing to compare the present results with photosynthetic ET in the purple bacterial reaction centers. As described in the Introduction, ET from $Bphe^{\bullet-}$ to the primary quinone, Q_A, loses ~0.6 eV out of the initial input energy (1.4 eV), which

(36) The residual absorbance observed at 660 nm in Figure 6b corresponds to the absorption due to $C_{60}^{\bullet-}$, which decays at a much slower rate, as shown in the time profile at 1000 nm.

(37) Ohta et al. suggested that photoinduced charge transfer occurs along the meso,meso-linked zincporphyrin arrays.[25a] Similar charge migration might take place in the zincporphyrin dimer moiety of Fc−$(ZnP)_2$−C_{60}.

(38) The total quantum yield of the charge separation (0.71) for Fc−$(ZnP)_2$−C_{60} in THF agrees largely with the corresponding value (0.63) obtained by the transient absorption spectra ($\epsilon = 4700$ M^{-1} cm^{-1} at 1000 nm).[22b]

is a disadvantage in terms of energy efficiency. However, if the driving force for ET from $Bphe^{\bullet-}$ to the primary quinone Q_A becomes much smaller, the stepwise CR process via intermediate states $(Bchl)_2^{\bullet+}Q_A^{\bullet-}$ and $(Bchl)_2^{\bullet+}Bphe^{\bullet-}$ would prevail over the extremely slow direct CR process from $Q_B^{\bullet-}$ to $(Bchl)_2^{\bullet+}$ (~1 s). Such an escape pathway via stepwise CR processes indeed takes place in the present system, because the direct CR from $C_{60}^{\bullet-}$ to Fc^+ ($k_{ET(CR2)} \sim 10^2\ s^{-1}$) would be too slow to compete with the stepwise processes ($\sim 10^4\ s^{-1}$). It should be noted here that such a switching of competing pathways occurs only in donor−acceptor arrays with small reorganization energies,[13] which make it possible to slow the direct CR process from the final CS state to the ground state.

In conclusion, we have prepared ferrocene-porphyrin dimer-fullerene triad where *meso,meso*-linked porphyrin dimer is incorporated successfully into a charge separation unit as a photosynthetic multistep ET model for the first time. The triad reveals photoinduced ET from the porphyrin dimer excited-singlet state to the C_{60}, followed by CSH from the ferrocene to the porphyrin dimer radical cation, to produce the ferricenium ion−C_{60} radical ion pair with a high quantum yield (~0.71−0.88) as well as a long-lived CS lifetime (~16−83 μs) depending on the solvent. It should be emphasized here that the CS lifetime of the present triad has been prolonged by replacing porphyrin monomer with porphyrin dimer without reducing the quantum yield significantly. The CS lifetime is governed by a rate-limiting ET from $(ZnP)_2$ to Fc^+ in $Fc^+-(ZnP)_2-C_{60}^{\bullet-}$, which is followed by a subsequent fast ET from $C_{60}^{\bullet-}$ to $(ZnP)_2^{\bullet+}$ to generate the ground state, $Fc-(ZnP)_2-C_{60}$.

Acknowledgment. This work was supported in part by Grants-in-Aid (Nos. 11228205, 13440216, and 13031059) and the Development of Innovative Technology (No. 12310) from the Ministry of Education, Culture, Sports, Science and Technology, Japan.

Supporting Information Available: Experimental details, including synthetic procedures and characterization (S1−S8) (8 pages, print/PDF). This material is available free of charge via the Internet at http://pubs.acs.org.

JA016655X

(39) The smaller activation energies (0.15−0.19 eV) relative to the difference in the energy levels (0.28−0.40 eV) may also be explained by superexchange-mediated CR from the $C_{60}^{\bullet-}$ to the Fc^+ moiety via a virtual state, $Fc-(ZnP)_2^{\bullet+}-C_{60}^{\bullet-}$.

(40) No characteristic absorption due to the $(ZnP)_2^{\bullet+}$ was detected as an intermediate species for the CR processes of $Fc^+-(ZnP)_2-C_{60}^{\bullet-}$. This also demonstrates that an intramolecular CR from $(ZnP)_2$ to Fc^+ is much slower than that from $C_{60}^{\bullet-}$ to $(ZnP)_2^{\bullet+}$.